Journal of Rock Mechanics and Geotechnical Engineering. 2010, 2 (2): 178–187

Journal of Rock Mechanics and Geotechnical Engineering

Journal online: www.rockgeotech.org

Finite element analysis of anchor plates using non-coaxial models

Yunming Yang[1*], H. S. Yu[2]

[1] *Institute of Rock and Soil Mechanics, Chinese Academy of Sciences, Wuhan, 430071, China*

[2] *Faculty of Engineering, University of Nottingham, Nottingham, NG7 2RD, UK*

Received 10 January 2010; received in revised form 28 April 2010; accepted 6 May 2010

Abstract: The non-coaxial model simulating the non-coincidence between the principal stresses and the principal plastic strain rates is employed within the framework of finite element method (FEM) to predict the behaviors of anchors embedded in granular material. The non-coaxial model is developed based on the non-coaxial yield vertex theory, and the elastic and conventional coaxial plastic deformations are simulated by using elasto-perfectly plastic Drucker-Prager yield function according to the original yield vertex theory. Both the horizontal and vertical anchors with various embedment depths are considered. Different anchor shapes and soil friction and dilation angles are also taken into account. The predictions indicate that the use of non-coaxial models leads to softer responses, compared with those using conventional coaxial models. Besides, the predicted ultimate pulling capacities are the same for both coaxial and non-coaxial models. The non-coaxial influences increase with the increasing embedment depths, and circular anchors lead to larger non-coaxial influences than strip anchors. In view of the fact that the design of anchors is mainly determined by their displacements, ignoring the non-coaxiality in finite element numerical analysis can lead to unsafe results.

Key words: finite element analysis; non-coaxial models; anchor plates; ultimate pulling capacities; principal stress rotations

1 Introduction

Anchor plates are widely used in geotechnical engineering to provide uplift resistance in transmission towers, sheet pile walls, buried pipelines, etc. There are various approaches to design and analyze anchor plates, which can be categorized into the limit equilibrium method, slip-line method, limit analysis and finite element method [1]. Each approach has its own strength and weakness. For example, most of designs are performed by using the limit equilibrium method due to its simplicity. However, the limit equilibrium method is purely static in nature and does not consider soil kinematics. In addition, in this method, the equilibrium and yield conditions are satisfied only in a global sense, and the static admissibility of the stress field is violated. Moreover, this method is based on many assumptions, such as the shapes of rupture surfaces in soil mass which vary with individual problems [2, 3]. In the method of slip-line fields, a yield condition is combined with the equations of equilibrium to give a set of differential equations at plastic equilibrium. From these basic equations, a slip-line network can be constructed and the collapse load is determined. As discussed by Chen [4], the conditions for static and kinematic admissibility are often difficult to be satisfied in this method. Examples using limit analysis in anchor analysis can be seen in Refs.[5–9]. Given a rigid plastic soil with an associated flow rule, the upper and lower bound theorems of limit analysis can be used to obtain rigorous bounding solutions for stability problems. These rigorous bounding solutions can be used to check the accuracy of other approximate solutions. In addition, it is difficult to construct statically admissible stress fields or kinematically admissible velocity fields by hand in this method. Moreover, its assumption of rigid plasticity cannot account for the effects of soil stress histories, layered soil profiles, and advanced soil models.

Examples using finite element method in anchor analysis can be seen in Refs.[10–12]. Unlike other methods, it is not restricted to the geometry of problems analyzed, and it can also consider complex soil profiles, loading histories, and advanced soil

Doi: 10.3724/SP.J.1235.2010.00178
*Corresponding author. Tel:+86-27-87198797;
E-mail: ymyang@whrsm.ac.cn
Supported by an EPSRC grant (GR/S29232/01) from the UK Government

models. Furthermore, it can not only predict collapse loads, but also give load-displacement curves. In the design of anchors, the main concern is their displacements under working loads, instead of collapse loads.

A soil constitutive model is an essential part in finite element predictions of geotechnical structures responses, including anchor behaviors. The accuracy of finite element predictions is largely dependent on the accuracy of models to represent soil behaviors [13]. Most of soil models applied to finite element predictions are coaxial models, in which the orientations of the principal stresses coincide with those of principal plastic strain rates. It is true if the directions of principal stresses do not change during loading. However, the orientations of the principal stresses and the principal plastic strain rates do not coincide if the principal stresses rotate during loading. This is verified by a large number of experimental results [14–17]. In these tests, a soil specimen is subjected to shearing which induces the principal stress rotations. The orientations of the principal stresses and the principal plastic strain rates are different during early stage of shearing in these tests, and they approach the same value with the increasing shear. A typical simple shear test result is shown in Fig.1, indicating the difference of orientations between the major principal stress and the strain rate

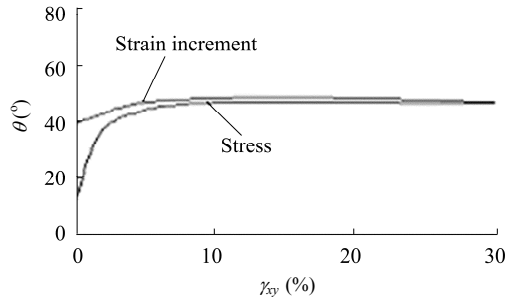

(a) $\sigma_y = 135$ kPa.

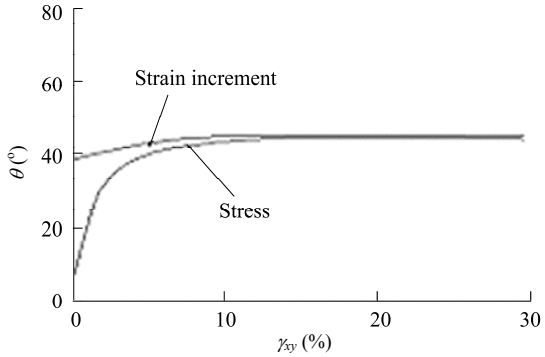

(b) $\sigma_y = 396$ kPa.

Fig.1 Experimental results showing principal stress and strain rate rotation against shear strain in the simple shear tests revised [4].

during a soil sample shearing which causes principal stress rotations [14]. Theoretical studies in micromechanics also support this argument [18]. Some non-coaxial models are developed to take into account the non-coaxiality, such as the double-shearing theories [19, 20], the combined plastic potential and double-shearing theories [21, 22], hypoplasticity theory [23] and the yield vertex theory proposed by Rudnicki and Rice [24]. However, these non-coaxial theories are mainly used to investigate the development of shear bands of granular materials, and considerable improvements are made by using the non-coaxial theories [25–27]. Besides, the influences of non-coaxial plasticity on stress-strain responses are rarely touched. Yu et al. [22, 28] made the initiative to comprehensively investigate the influences of non-coaxial models on the stress-strain response of a granular material sample by simulating its simple shear behavior. Their predictions indicate that a non-coaxial model generally gives a softer response than a coaxial model does. The difference in coaxial and non-coaxial predictions increases with increasing principal stress rotation in simple shear simulations, and the inclusion of non-coaxial plastic strain rates cannot be neglected when a sample experiences a large amount of principal stress rotations. The preliminary predictions using non-coaxial plasticity in footing analysis [29, 30] substantiate the argument in simple shear simulations.

It is evident that the soil mass experiences large shear and principal stress rotations in anchor problems. This paper aims at investigating the influences of non-coaxial models on the predictions of anchor behavior. The yield vertex non-coaxial theory [24] is used, which is developed based on conventional plasticity. In accordance with the original yield vertex theory, elasto-perfectly plastic Drucker-Prager yield function is employed to represent the elastic and conventional coaxial plastic deformations of granular material. Both horizontal and vertical anchors are considered with different embedment depths. In addition, different anchor shapes, soil frictions and dilation angles are also taken into account.

2 The non-coaxial constitutive model and its finite elements implementation

According to elasto-plasticity theory, the total strain rate is composed of an elastic and a plastic components:

$$\dot{\varepsilon}_{ij} = \dot{\varepsilon}_{ij}^{\mathrm{e}} + \dot{\varepsilon}_{ij}^{\mathrm{p}} \tag{1}$$

where the superscripts "e" and "p" denote the elastic and plastic components, respectively. $\dot{\varepsilon}^{\mathrm{e}}$ is linked to stress rate $\dot{\sigma}$ by

$$\dot{\sigma}_{ij} = E_{ijkl}\,\dot{\varepsilon}^{\mathrm{e}}_{kl} \tag{2}$$

$$E_{ijkl} = K\delta_{ij}\delta_{kl} + G\left(\delta_{ik}\delta_{jl} + \delta_{il}\delta_{jk} - \frac{2}{3}\delta_{ij}\delta_{kl}\right) \tag{3}$$

where K and G are the elastic bulk and shear moduli, respectively; and δ_{ij} is the Kronecker delta. In non-coaxial plasticity theory, $\dot{\varepsilon}^{\mathrm{p}}$ is composed of a coaxial and non-coaxial parts, denoted with $\dot{\varepsilon}^{\mathrm{pc}}$ and $\dot{\varepsilon}^{\mathrm{pn}}$, respectively, given as

$$\dot{\varepsilon}^{\mathrm{p}}_{ij} = \dot{\varepsilon}^{\mathrm{pc}}_{ij} + \dot{\varepsilon}^{\mathrm{pn}}_{ij} \tag{4}$$

where $\dot{\varepsilon}^{\mathrm{pc}}$ can be determined according to conventional plasticity theory, and $\dot{\varepsilon}^{\mathrm{pn}}$ is determined according to the yield vertex theory proposed by Rudnicki and Rice [24].

The determination of $\dot{\varepsilon}^{\mathrm{pc}}$ is described first followed by that of $\dot{\varepsilon}^{\mathrm{pn}}$. The yield vertex theory is developed on the basis of a modified Drucker-Prager yield function, and perfect plasticity is assumed. The modified Drucker-Prager yield function can be written in general stress space as

$$f = \sqrt{(a\sin\varphi)^2 + \tau^2} - p\sin\varphi - c\cos\varphi \tag{5}$$

where $\tau = \sqrt{0.5(s_{ij}s_{ij})}$ and s_{ij} represents the deviatoric stress tensor; p is the mean normal stress; c denotes the soil cohesion and is chosen close to zero for granular materials in this paper; φ stands for the friction angle in perfect plasticity; and the parameter a is used to round the apex of the original Drucker-Prager yield function to avoid the singularity problem. When $a \le 0.5c\cot\varphi$, the modified Drucker-Prager yield function closely represents the original one. The plastic potential is the same as the yield function except that φ is replaced by dilation angle ψ whenever a non-associated flow rule is used.

Following Rudnicki and Rice [24], the non-coaxial plastic strain rate is defined as

$$\dot{\varepsilon}^{\mathrm{pn}}_{ij} = \frac{1}{h_{\mathrm{nc}}} n_{ij} \tag{6}$$

$$n_{ij} = \dot{s}_{ij} - \frac{s_{ij}s_{kl}}{2\tau^2}\dot{s}_{kl} \tag{7}$$

where h_{nc} represents the non-coaxial plastic modulus and is assumed to be a constant for simplicity. From the above non-coaxial formulations, it can be seen that when $\dot{s}_{kl}$ and s_{kl} are in the same direction, n_{ij} is zero and the non-coaxial plastic strain rates vanish. Equations (6) and (7) also show that $\dot{\varepsilon}^{\mathrm{pn}}$ is defined merely on deviatoric plane. Correspondingly, there are only deviatoric plastic non-coaxial strains, and the volumetric plastic strain is entirely coaxial. Figure 2 schematically shows the coaxial and non-coaxial plastic strain rates on the deviatoric plane. While the coaxial part of plastic strain rate is normal to the yield surface, the non-coaxial part is tangential to the yield surface. It is the tangential component that makes the principal stress orientation different from the orientation of plastic strain rate. $\dot{\varepsilon}^{\mathrm{pn}}$ can be linked to total stress rates, given as

$$\dot{\varepsilon}^{\mathrm{pn}}_{ij} = \frac{1}{h_{\mathrm{nc}}} N_{ijkl}\dot{\sigma}_{kl} \tag{8}$$

$$N_{ijkl} = \frac{1}{2}\left(\delta_{ik}\delta_{jl} + \delta_{il}\delta_{jk} - \frac{2}{3}\delta_{ij}\delta_{kl} - \frac{s_{ij}s_{kl}}{\tau^2}\right) \tag{9}$$

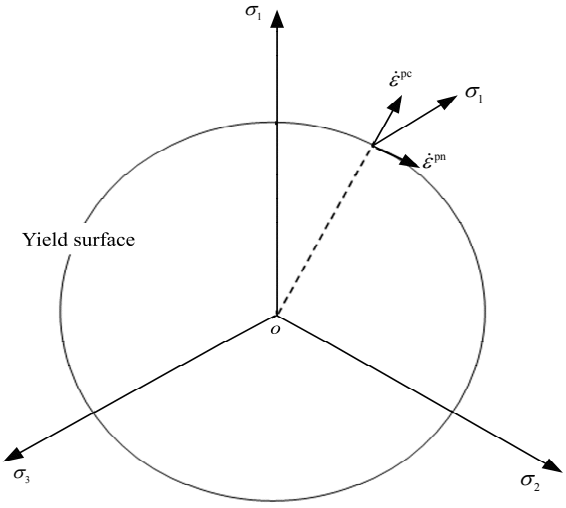

Fig.2 Schematic diagram of coaxial and non-coaxial plastic strain rates on the deviatoric plane.

One can further obtain the relationship between total strain rate and stress rate, given as

$$\dot{\sigma}_{ij} = \left(E_{ijkl} - \frac{E_{ijab}R_{ab}E_{klcd}l_{cd}}{K_p + l_{mn}E_{mnst}R_{st}} - \frac{4G^2}{h_{\mathrm{nc}} + 2G}N_{ijkl}\right)\dot{\varepsilon}_{kl} \tag{10}$$

It can be seen that the first two terms on the right side of Eq.(10) are contributed by elastic and coaxial plastic strain rates, and the third term reflects the influences of non-coaxial plastic strain rates. Equation (10) also shows that the influences of non-coaxial models are dependent on the ratio of h_{nc} to G. Smaller values of h_{nc}/G give greater non-coaxial influences.

The above constitutive formulations are implemented into a finite element software ABAQUS as a user-

defined subroutine. A Newton-Raphson algorithm is used to solve nonlinear finite element equations in ABAQUS. In the material subroutine, an explicit sub-stepping scheme with automatic error control is used to integrate the constitutive formulations [31–34]. Given a strain increment passed down from the main program, the strain increment is divided into multiple sub-increments. In each sub-increment, the constitutive equations are integrated by using both Euler scheme, which is of first order accuracy, and modified Euler scheme, which is of second order accuracy. The local error of numerical integrations is found by taking the difference of the integration results using these two schemes. Once the local error is computed for a given sub-increment, the size of the next sub-increment is determined by extrapolation of the current error compared with the prescribed error tolerance. Therefore, this scheme can automatically divide the imposed strain increment according to the prescribed error tolerance. For a detailed description of the formulations and their numerical solutions, readers can refer to Ref.[28].

To show the non-coaxial influences on the presence of principal stress rotations, the above non-coaxial finite element procedure is employed to simulate the response of a soil sample subjected to simple shearing. The simple shearing causes the rotation of principal stresses. An 8-noded bi-quadratic element with a reduced integration is employed to represent the soil sample, and all the sides of the element remain linear and parallel to their original ones throughout the loading. The elastic modulus of soil is 10 MPa and its Poisson's ratio is 0.3. Its friction angle, φ, is 30°, and the associated flow rule is assumed. The initial static lateral pressure coefficient, K_0, is 0.5. Two values of non-coaxial moduli ratio are examined: $h_{nc}/G = 0.5$ and 0.2. While the soil is subjected to a constant vertical stress of 100 kPa, a shear strain is gradually applied until the failure of soil. Figure 3 shows the predicted responses, including stress-strain responses and the orientations of the major principal stress and the strain rate. The responses are first in the elastic regime, characterized with very small and neglected deformation. 20° of principal stress rotation takes place in the elastic regime. The responses quickly enter the plastic regime, and the principal stress rotates from 20° to 60° in the plastic regime. The difference of predictions between the coaxial and non-coaxial models can be seen in the plastic regime. When the non-coaxial models are used, the orientation of the major principal plastic strain rate is different from that of the principal stress, and the former is ahead of the latter. The use of non-coaxial model also gives a softer response during the early stage of loading, compared with that using the coaxial model. A smaller value of

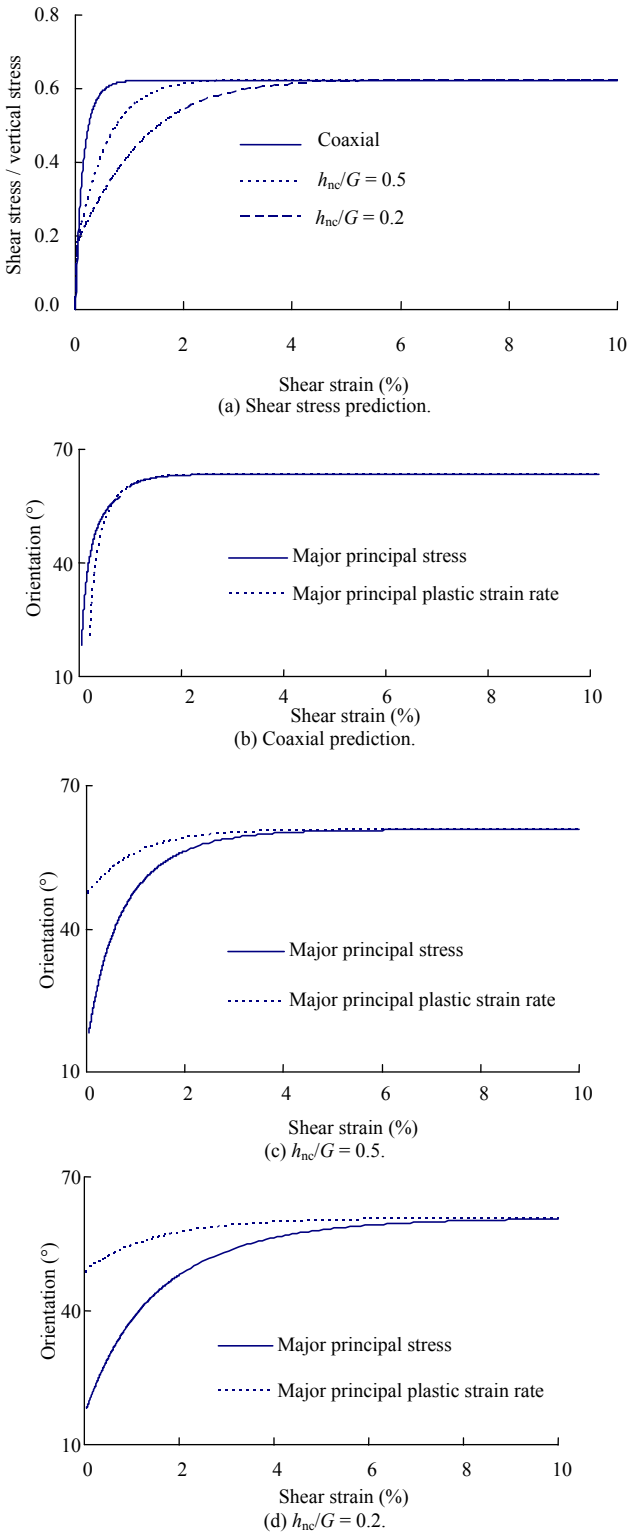

Fig.3 The simulations of simple shear behaviors by using the coaxial and non-coaxial models.

h_{nc}/G gives a larger non-coaxial influence. Furthermore, regardless of the coaxial or non-coaxial models, all the predictions approach the same ultimate values with increasing shear strain. The predicted difference of orientations between major principal stress and plastic strain rate is the same as in the typical simple shear test results in Fig.1.

3 Numerical simulations of anchor plates

The properties of soil are chosen to be the same as those in the above simple shear simulations. In addition to the coaxial model for soil, two non-coaxial moduli are considered: h_{nc}/G = 0.5 and 0.2. The soil element is an 8-noded bi-quadratic plane strain element with reduced integration. The unit weight of soil γ is 18 kN/m^3, and the initial vertical stress of soil mass is determined according to its gravity. Both horizontal and vertical strip anchor plates are considered, and the anchors are assumed to be smooth and rigid. They are embedded at different depths below the ground surface. The width of anchor B is 2 m, and h represents the depth where it is buried. Three cases are considered, h/B=1, 3, and 8, representing the low, medium and deep depths, respectively. The interfaces between anchors and soil are modeled by using the contact elements provided in ABAQUS. These contact elements can only transmit compression and they immediately break away whenever tension is about to develop. Figure 4 illustrates the finite elements meshes for deep horizontal and vertical anchor plates. To simulate the loading of anchors, vertical or horizontal displacement

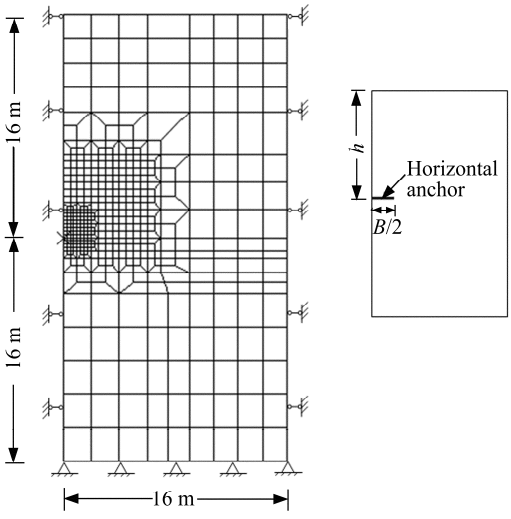

(a) Horizontal anchor.

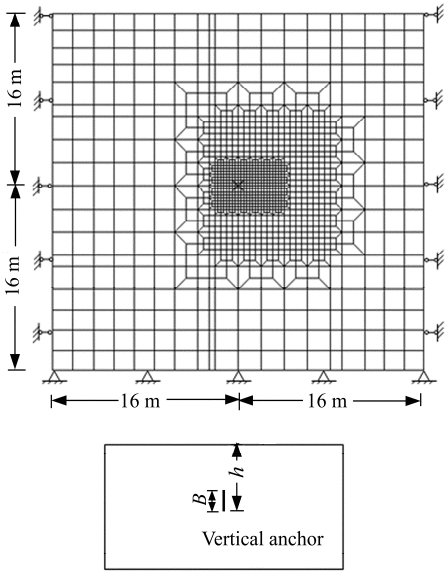

(b) Vertical anchor.

Fig.4 Finite element meshes for deep anchors.

is imposed to rigid anchors until the failure of soil mass. The force applied to anchors is determined from the pressure on the contact surfaces between soils and anchors. To verify the user-developed model subroutine, the predictions by using the user-developed coaxial model subroutine are compared with those by using the model provided in ABAQUS, and they give the same results.

Figure 5 shows the predicted load-displacement curves for the horizontal anchor plates embedded at different depths by using both coaxial and non-coaxial models. Figure 6 shows the predictions for the vertical anchors. In these two figures, x-axis denotes the displacement of anchors normalized by their width, and y-axis denotes the pressure on the anchors normalized by γh. As expected, Fig.5 shows that deep anchors give larger normalized ultimate pulling capacities than shallow anchors do. Figures 5 and 6 also indicate that the use of non-coaxial models gives softer responses compared with the coaxial models. With the increase in load, the coaxial and non-coaxial predictions approach the same ultimate values. These features are the same as those in simple shear simulations. Similar to the simple shear simulations, the differences between coaxial and non-coaxial predictions result from the rotation of the principal stresses in the soil mass. Figure 7 shows the magnitude and orientation of the major principal stress in the soil mass at the end of loading for the deep horizontal and

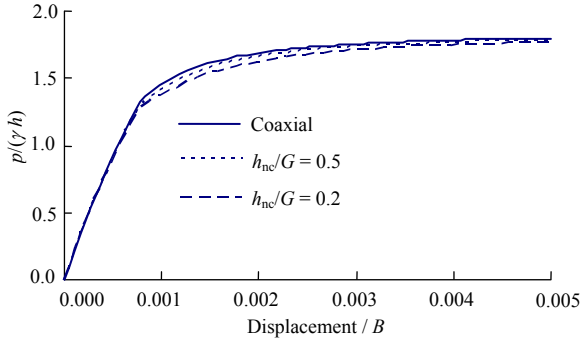

(a) $h/B = 1$.

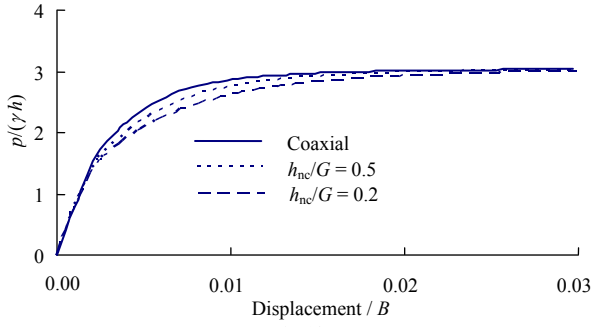

(b) $h/B = 3$.

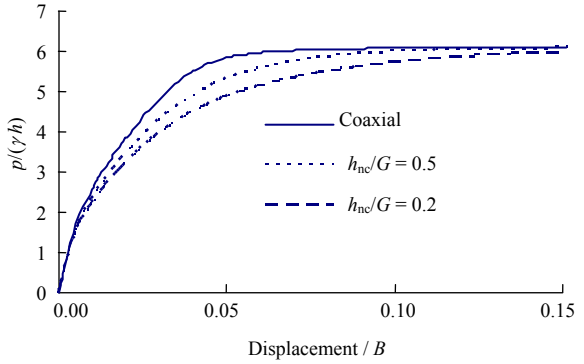

(c) $h/B = 8$.

Fig.5 The predicted load-displacement curves of horizontal anchor plates.

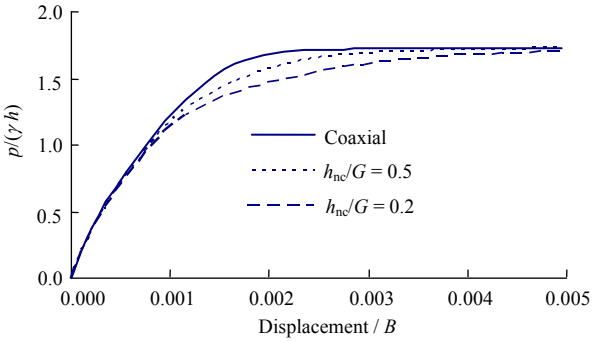

(a) $h/B = 1$.

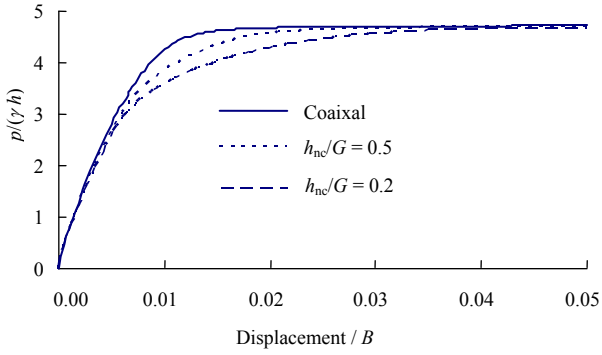

(b) $h/B = 3$.

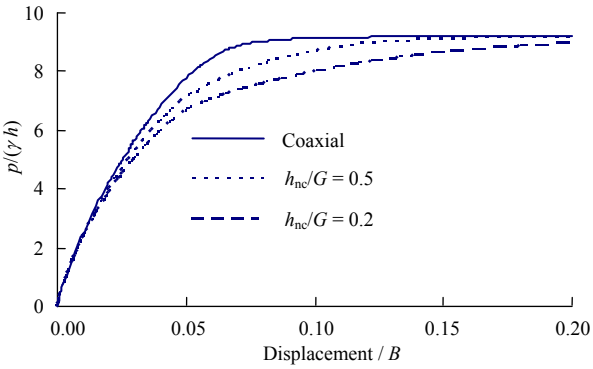

(c) $h/B = 8$.

Fig.6 The predicted load-displacement curves of vertical anchor plates.

vertical anchors. In this figure, the principal stresses undergo a large amount of rotations. The most significant area of the principal stress rotations starts with the edge of anchors and extends outward. Figures 5 and 6 indicate that the non-coaxial influences increase with the increasing embedment depth of anchors, and this is the most noticeable for horizontal anchors. This is because the shallow horizontal anchors quickly approach failure after the start of loading, and the soil mass rarely undergoes plastic deformation before the anchors reach their ultimate bearing capacities. This can be seen in Fig.5(a), where the load-displacement curves of shallow-buried anchors

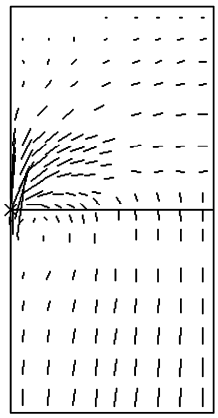

(a) Horizontal anchor.

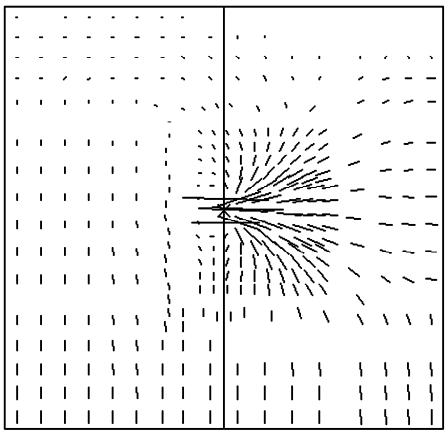

(b) Vertical anchor.

Fig.7 Major principal stress rotations of deep anchors.

exhibit brittle features. From the non-coaxial formulations, the non-coaxial plastic strain takes place in companion with the coaxial plastic strain, and this brittle behavior of shallow-burried anchors circumvents the non-coaxial influences.

Figure 8 shows the non-coaxial influences with different soil friction angles. The same deep horizontal anchor as in the above analysis is employed except that the friction angles of soil are chosen to be 26° and 34°, respectively. The associated flow rule is still assumed. Comparing the behaviors of anchors with different friction angles (26°, 30°, 34°), one can see that a smaller friction angle leads to a larger non-coaxial influence. In addition, the non-coaxial influences come into effect earlier for the smaller friction angle than that for the larger one. This feature is important because the displacement of an anchor rather than its ultimate pulling capacity is the major concern in practical designs. The reason is that, given K_0 equals 0.5, the initial stress state of soil is on the yield surface when φ is 26°. Therefore, the non-coaxial plastic deformation takes place in companion with the conventional coaxial plastic deformation immediately after the soil is loaded. For larger friction angles, the stress path has to travel in the purely elastic regime for some distance before it reaches the plastic state. Correspondingly, a large part of principal stress rotation takes place in the elastic regime, which does not induce non-coaxial plastic deformations.

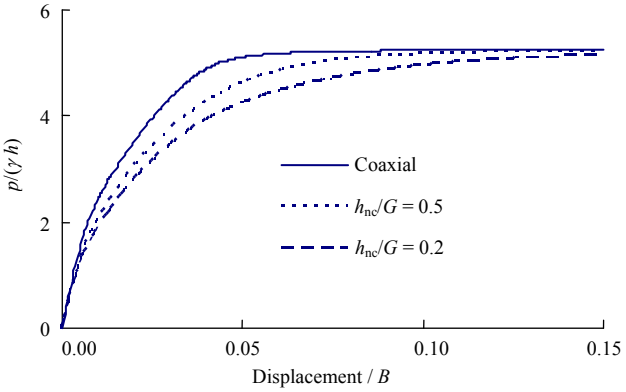

(a) $\varphi = 26°$.

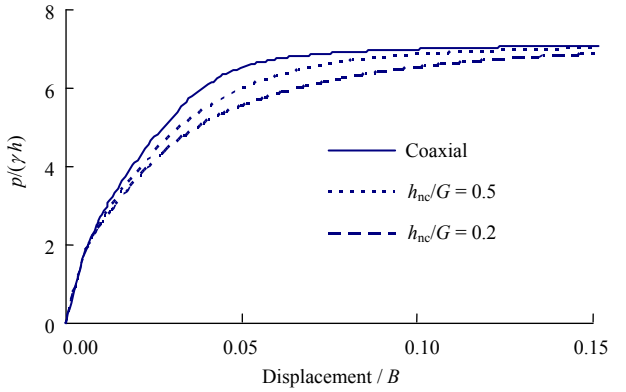

(b) $\varphi = 34°$.

Fig.8 The predicted load-displacement curves for deep horizontal anchors with different friction angles.

Figure 9 shows the predictions of anchor behaviors when the non-associated flow rule is used for soil. The same deep horizontal anchor as in the above analysis is considered, except that the dilation angle of soil is chosen to be 15°, compared with its friction angle of 30°. This smaller dilation angle is used to represent the behavior of loose sand. It should be noted that the dilation angle can not be chosen too small in this analysis, due to the restriction of singularity problems resulted from non-associated flow rules in finite element analysis. Comparing the predictions by using associated and non-associated flow rules, one can see that the use of non-associated flow rule gives a smaller

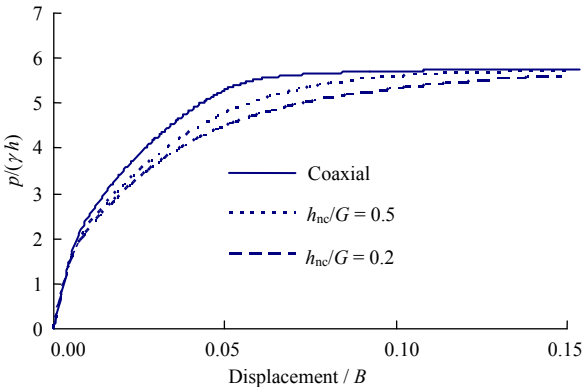

Fig.9 The predicted load-displacement curves of deep horizontal anchor with a non-associated flow rule (ψ=15°, φ = 30°).

ultimate pulling capacity. In addition, the non-coaxial model has the same influences regardless of flow rules.

All the above studies are performed for smooth anchors. The non-coaxial influences are also investigated when the surface of anchors is rough. Due to the axisymmetric nature of horizontal anchors, the roughness of anchors does not greatly influence their behaviors. Previous study indicates that the roughness of anchors plays a great role in shallow vertical anchors. Figure 10 shows the predictions of rough vertical anchor with h / B =1 by using the coaxial and non-coaxial models. All the conditions are the same as in the smooth anchor except that the interface between anchor and soil is assumed to be rough. The interface friction angle is the same as that in soil with φ = 30°. Comparing the load-displacement curves between the smooth and rough anchors, one can see that the ultimate pulling capacity increases with the interface friction. Moreover, the non-coaxial influences are also greater in the rough anchor than those in the smooth anchor. This can be attributed to different areas of soil mass involving principal stress rotations for the smooth and rough anchors. On one hand, the pulling of both anchors results in a shear zone starting with the anchor edge and extending outward. On the other hand, right in front of the smooth anchor, the soil mass is only subjected to the increase in horizontal stress. In addition to the increase in horizontal stress, the soil mass in front of the rough anchor is subjected to shearing resulted from the friction between the anchor surface and soil. Correspondingly, the larger area of the soil mass involving the principal stress rotations results in larger non-coaxial influences for the rough anchor.

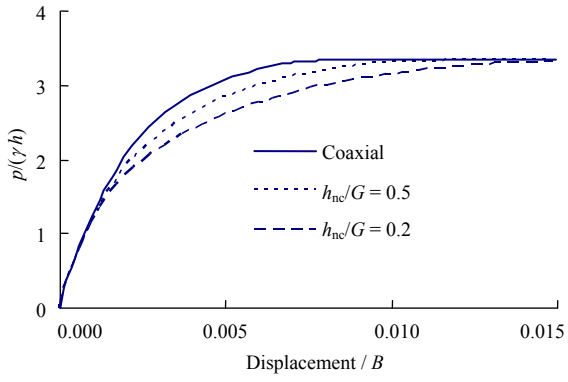

Fig.10 The predicted load-displacement curves of the shallow vertical anchor with a rough surface.

While all the above analyses are performed on strip anchors, the non-coaxial influences on the behaviors of circular anchors are investigated in this section. The same soil and loading conditions as in strip anchors are assumed except that the 8-noded bi-quadratic plane strain soil elements with reduced integration are replaced by the 8-noded axisymmetric elements with reduced integration. In order to avoid the over-constrained problems, the horizontal anchors only with low and medium embedment depths are considered. Figure 11 shows the predictions of the behaviors of circular horizontal anchors. Comparing the predictions of strip and circular anchors, one can see that the non-coaxial influences are much larger in the latter than those in the former. It is obvious that the shearing to the soil mass originates from the edge of an anchor. Given the radius of the circular anchor and the half width of the strip anchor are both 1 m, the ratios of the circumference to the area of the circular anchor are 2, and 1 for the strip anchor, respectively. Correspondingly, the soil mass above the circular anchor experiences larger shear and leads to greater non-coaxial effects than those above the strip anchor.

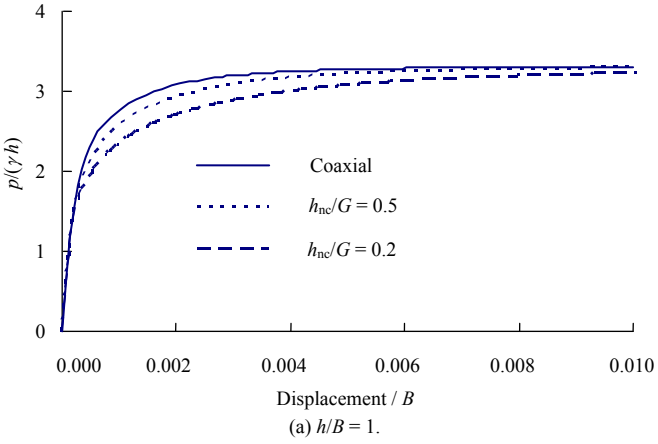

(a) h/B = 1.

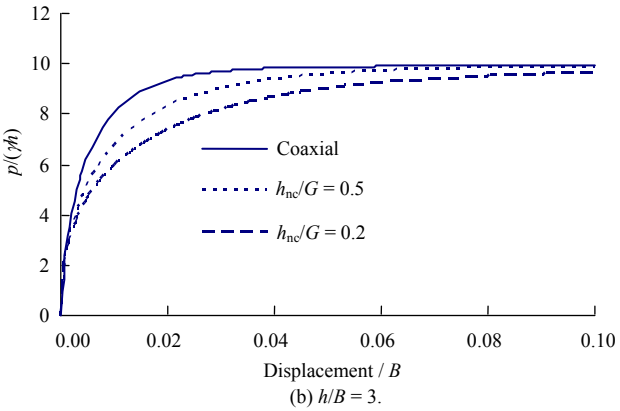

(b) h/B = 3.

Fig.11 The predicted load-displacement curves of the circular horizontal anchor.

4 Conclusions

The influences of non-coaxial models on the predictions of anchor behaviors within the framework of FEM are comprehensively investigated in this paper. The non-coaxial model is developed based on the non-coaxial yield vertex theory proposed by Rudnicki and Rice [24], and the elastic and conventional coaxial plastic deformations are simulated by using the elasto-perfectly plastic Drucker-Prager yield function. Both horizontal and vertical anchors with different embedment depths are simulated. Considerations are also given to different anchor shapes, anchor roughnesses, frictions and dilation angles of soils. All the predictions indicate that the use of non-coaxial models gives softer responses than those using coaxial models. Besides, the predicted ultimate pulling capacities are the same by using the coaxial and non-coaxial models. This softer response by using the non-coaxial model is attributed to the principal stress rotations of soil mass. The predictions also indicate that the non-coaxial model has a larger influence on deep anchors than that on shallow-burried anchors, because shallow-burried anchors feature brittle responses. In addition, circular anchors induce larger non-coaxial influences than the strip anchors because of the larger ratio of anchor circumference to area in the former than that in the latter.

References

[1] Das B M. Earth anchors. [S.l.]: Elsevier Science Publishers, 1990.

[2] Chattopadhyay B C, Pise P J. Breakout resistance of horizontal anchors in sand. Soils and Foundations, 1986, 26 (4): 16–22.

[3] Ilamparuthi K, Muthukrishnaiah K. Anchors in sand bed: delineation of rupture surface. Ocean Engineering, 1999, 26 (12): 1 249–1 273.

[4] Chen W F. Limit analysis and soil plasticity. [S.l.]: Elsevier Science Publishers, 1975.

[5] Murray E J, Geddes J D. Uplift of anchor plates in sand. Journal of Geotechnical Engineering, 1987, 113 (3): 202–215.

[6] Murray E J, Geddes J D. Resistance of passive inclined anchors in cohesionless medium. Geotechnique, 1989, 39 (3): 417–431.

[7] Kumar J. Upper bound solution for pullout capacity of anchors on sandy slopes. International Journal for Numerical and Analytical Methods in Geomechanics, 1997, 21 (7): 477–484.

[8] Merifield R S, Sloan S W, Yu H S. Stability of plate anchors in undrained clay. Geotechnique, 2001, 51 (2): 141–153.

[9] Merifield R S, Lyamin A V, Sloan S W, et al. Three-dimensional lower bound solutions for stability of plate anchors in clay. Journal of Geotechnical and Geoenvironmental Engineering, 2003, 129 (3): 243–253.

[10] Rowe R K, Davis E H. Behavior of anchor plates in clay. Geotechnique, 1982, 32 (1): 9–23.

[11] Rahman M A, Othman M A, Edil T B. Effect of plate flexibility on behavior of shallow anchors. Soils and Foundations, 1992, 32 (3): 137–143.

[12] Thorne C P, Wang C X, Carter J P. Uplift capacity of rapidly loaded strip anchors in uniform strength clay. Geotechnique, 2004, 54 (8): 507–517.

[13] Yu M H, Xia G Y, Kolupaev V A. Basic characteristics and development of yield criteria for geomaterials. Journal of Rock Mechanics and Geotechnical Engineering, 2009, 1 (1): 71–88.

[14] Roscoe K H. The influence of strains in soil mechanics. Geotechnique, 1970, 20 (2): 129–170.

[15] Oda M, Konishi J. Microscopic deformation mechanism of granular material in simple shear. Soils and Foundations, 1974, 14 (4): 25–38.

[16] Ishihara K, Towhata I. Sand response to cyclic rotation of principal stress direction as induced by wave loads. Soils and Foundations, 1983, 23 (4): 11–16.

[17] Joer H A, Lanier J, Fahey M. Deformation of granular material due to rotation of principal axes. Geotechnique, 1998, 48 (5): 605–619.

[18] Christofferson J, Mehrabadi M M, Nemat-Nasser S. A micro-mechanical description of granular material behavior. Journal of Applied Mechanics, 1981, 48 (2): 339–344.

[19] Spencer A J M. A theory of the kinematics of ideal soils under plane strain conditions. Journal of Mechanics and Physics of Solids, 1964, 12 (5): 337–351.

[20] De Josselin De Jong G. The double-sliding, free-rotating model for

granular assemblies. Geotechnique, 1971, 21 (2): 155–163.

[21] Harris D. Constitutive equations for planar deformations of rigid-plastic materials. Journal of the Mechanics and Physics of Solids, 1993, 41 (9): 1 515–1 531.

[22] Yu H S, Yuan X. On a class of non-coaxial plasticity models for granular soils. In: Proceedings of the Royal Society of London (Series A). [S.l.]: [s.n.], 2006: 725–748.

[23] Kolymbas D. An outline of hypoplasticity. Archive Applied Mechanics, 1991, 61 (3): 143–151.

[24] Rudnicki J W, Rice J R. Conditions for the localisation of deformation in pressure-sensitive dilatant materials. Journal of the Mechanics and Physics of Solids, 1975, 23 (6): 371–394.

[25] Papamichos E, Vardoulakis I. Shear band formation in sand according to non-coaxial plasticity model. Geotechnique, 1995, 45 (4): 649–661.

[26] Hashiguchi K, Tsutsumi S. Elastoplastic constitutive equation with tangential stress rate effect. International Journal of Plasticity, 2001, 17 (1): 117–145.

[27] Hashiguchi K, Tsutsumi S. Shear band formation analysis in soils by the subloading surface model with tangential stress rate effect. International Journal of Plasticity, 2003, 19 (10): 1 651–1 677.

[28] Yang Y, Yu H S. Numerical simulations of simple shear with non-coaxial soil models. International Journal for Numerical and Analytical Methods in Geomechanics, 2006, 30 (1): 1–19.

[29] Yu H S, Yuan X. The importance of accounting for non-coaxial behavior in modeling soil-structure interaction. In: Proceedings of the 11th IACMAG. Torino: [s.n.], 2005: 709–718.

[30] Yu H S, Yang Y, Yuan X. Application of non-coaxial plasticity models in geotechnical analysis. In: Proceedings of the 16th International Conference on Soil Mechanics and Geotechnical Engineering. Osaka, Japan: [s.n.], 2005: 993–996.

[31] Sloan S W. Substepping schemes for the numerical integration of elastoplastic stress-strain relations. International Journal for Numerical Methods in Engineering, 1987, 24 (5): 893–911.

[32] Abbo A J. Finite element algorithms for elastoplasticity and consolidation. PhD Thesis. Callaghan NSW, Australia: University of Newcastle, 1997.

[33] Yu Long, Liu Jun, Kong Xianjing. Stability of plate anchors in NC clay. Rock and Soil Mechanics, 2007, 28 (7): 1 427–1 434 (in Chinese).

[34] Rowe R K, Davis E H. Behavior of anchor plates in sand. Geotechnique, 1982, 32 (1): 25–41.